Ore Geology Reviews 64 (2015) 187–199

Contents lists available at ScienceDirect

Ore Geology Reviews

journal homepage: www.elsevier.com/locate/oregeorev

Large celestine orebodies formed by early-diagenetic replacement of gypsified stromatolites (Upper Miocene, Montevive–Escúzar deposit, Granada Basin, Spain)

Javier García-Veigas [a,*], Laura Rosell [b], Dioni I. Cendón [c,d], Luis Gibert [b], José M. Martín [e], José Torres-Ruiz [f], Federico Ortí [b]

[a] CCiTUB Scientific and Technological Centers, Universitat de Barcelona, 08028 Barcelona, Spain
[b] Departament de Geoquímica, Petrologia i Prospecció Geològica, Universitat de Barcelona, 08028 Barcelona, Spain
[c] Australian Nuclear Science and Technology Organization, Kirrawee DC, NSW 2322, Australia
[d] Connected Waters Initiative, School of BEES, UNSW, Sydney, NSW 2052, Australia
[e] Departamento de Estratigrafía y Paleontología, Universidad de Granada, 18071 Granada, Spain
[f] Departamento de Mineralogía y Petrología, Universidad de Granada, 18071 Granada, Spain

ARTICLE INFO

Article history:
Received 24 April 2014
Received in revised form 17 June 2014
Accepted 9 July 2014
Available online 15 July 2014

Keywords:
Celestine
Evaporites
$^{87}Sr/^{86}Sr$
Sulfate isotopes
Upper Miocene

ABSTRACT

The Montevive and the Escúzar stratabound celestine orebodies in the Upper Miocene evaporite succession of the intramontane Granada Basin (Spain) constitute one of the largest strontium deposits in the world. Celestine occurs within a gypsum/anhydrite–halite evaporite sequence where it replaces gypsum and gypsified stromatolites preserving carbonate peloids. $^{87}Sr/^{86}Sr$ and $\delta^{34}S$ values in the Montevive celestine deposit are close to those reported for the saline unit (Chimeneas Halite; marine to nonmarine) but higher than those of the overlying gypsum unit (Agrón Gypsum; nonmarine). $^{87}Sr/^{86}Sr$ and $\delta^{34}S$ isotope values in the Escúzar celestine deposit match the nonmarine values recorded in the upper part of the Agrón Gypsum. The similarity in isotope values between celestine and the corresponding gypsum host in the Escúzar deposit points to early-diagenetic mineralization. According to that, both orebodies are diachronous. Gypsum pseudomorphs and molds, intraformational breccias and karst structures in these celestine deposits point to dissolved gypsum as the main sulfate source. Diagenetic–hydrothermal $CaCl_2$ brines are interpreted to be the main strontium source. The spatial relationship between gypsified stromatolites and the ore deposits suggests the existence of coeval thermal springs related to fractures, bordering the saline lake. The proposed model envisages gypsum dissolution by SO_4^{2-}-poor and Sr^{2+}-rich, $CaCl_2$ diagenetic–hydrothermal water discharging in coastal ponds at times of dry periods and low meteoric water inflow. The increase in SO_4^{2-} concentration by gypsum dissolution and the low solubility of $SrSO_4$ would lead to celestine precipitation replacing gypsum and gypsified stromatolites.

1. Introduction

Celestine ($SrSO_4$) is a common minor mineral in modern and ancient marine sediments and in some lacustrine evaporites. There are even marine planktonic protozoan organisms (the *Acantharia*) that precipitate celestine shells biogenically (Bernstein et al., 1987; Deckker, 2004). The limited amount of celestine in marine sediments agrees with the low concentration of Sr^{2+} in modern seawater due to the low solubility of strontium sulfate. Although celestine is expected to precipitate during evaporation of seawater (Braitsch, 1971; Zherebstova and Volkova, 1966) it never forms significant accumulations. However, the largest known celestine orebodies are hosted in shallow-water carbonates and evaporites, commonly interfingering with clastic sediments (Hanor, 2004). Based on their relationships with associated sedimentary successions and their stable isotope geochemistry, two principal mechanisms for the formation of massive celestine ore deposits have been proposed (Hanor, 2000, 2004): 1) a syngenetic mechanism with primary precipitates derived from evaporated seawater, and 2) a diagenetic (epigenetic) replacement of carbonates and sulfate evaporites.

All large celestine orebodies are related to evaporite deposits: the Upper Permian of East Greenland (Scholle et al., 1990), the Lower Cretaceous deposits in Argentina's Neuquen Basin (Brodtkorb et al., 1982), and in the Sabinas Basin of Mexico (González-Sánchez et al.,

* Corresponding author. Tel.: +34 934021701; fax: +34 934021398.
E-mail address: garcia_veigas@ub.edu (J. García-Veigas).

http://dx.doi.org/10.1016/j.oregeorev.2014.07.009
0169-1368/

2009; Kesler and Jones, 1981), and the Cenozoic Ulas-Sivas Basin deposits of Central-Eastern Turkey (Tekin et al., 2001, 2002). Smaller replacements of Ca-sulfate evaporites by celestine in non-economic deposits have been described elsewhere (Carlson, 1987; Dill et al., 2009; Olaussen, 1981; Taberner et al., 2002; West, 1960; Wood and Shaw, 1976).

The Miocene Montevive–Escúzar deposit (Granada, Spain), with an annual production up to 200,000 tons of almost pure celestine, is the second largest known strontium deposit in the world after the Sabinas deposit of Mexico. The Montevive–Escúzar deposit is characterized by: 1) stratabound orebodies hosted by gypsum evaporites; 2) evidence of subaerial exposure (intraclastic breccias and karstic cavity fillings); 3) location in specific sites of the basin, generally along the margins and in local shoals; and 4) celestine formation followed by precipitation of calcite cement (Martín et al., 1984).

Taking into account the poor efficiency of $SrSO_4$-transport in solution, the understanding of the build-up of these large celestine deposits, particularly in a sedimentary context as occurs in the Granada Basin, requires the integrated study of the orebodies and the host sedimentary succession. The aim of this work is to propose a genetic model for the Montevive–Escúzar celestine deposit which could be applicable to other similar ore deposits.

2. Geological setting

The Betic Chain (southern Spain) and the Rif Mountains (in northern Africa) constitute the western portion of the Alpine peri-Mediterranean Orogenic belt, which formed as a result of the closure of the Tethys Ocean during Africa–Eurasia plate convergence. From the Late Miocene onward, an extensional regime was imposed, resulting in a group of postorogenic intramontane basins, referred to as 'Neogene Basins'. The Granada Basin (Fig. 1), situated in the center of the Betic Chain, at the western foot of the Sierra Nevada, is filled with Neogene and Pleistocene sediments unconformably overlying fault-controlled basement rocks. The basement consists of Paleozoic metamorphic rocks and Triassic carbonates in the southeastern half of the basin (Betic Internal Zone) and Mesozoic sedimentary rocks in the northwestern half (Betic External Zone). The main E–W directed fault-system in the basin (Rodríguez-Fernández and Sanz de Galdeano, 2006) is related to the major crustal Cádiz–Alicante Fault oriented NE–SW (Sanz de Galdeano, 2008) which affects the whole of the Betic Chain. A second NW–SE directed fault system cuts and displaces the previous one and defines the main areas of present-day basin subsidence.

The Neogene infilling of the Granada Basin (Braga et al., 1990, 2003; Corbí et al., 2012; Dabrio et al., 1982; Martín et al., 1984;

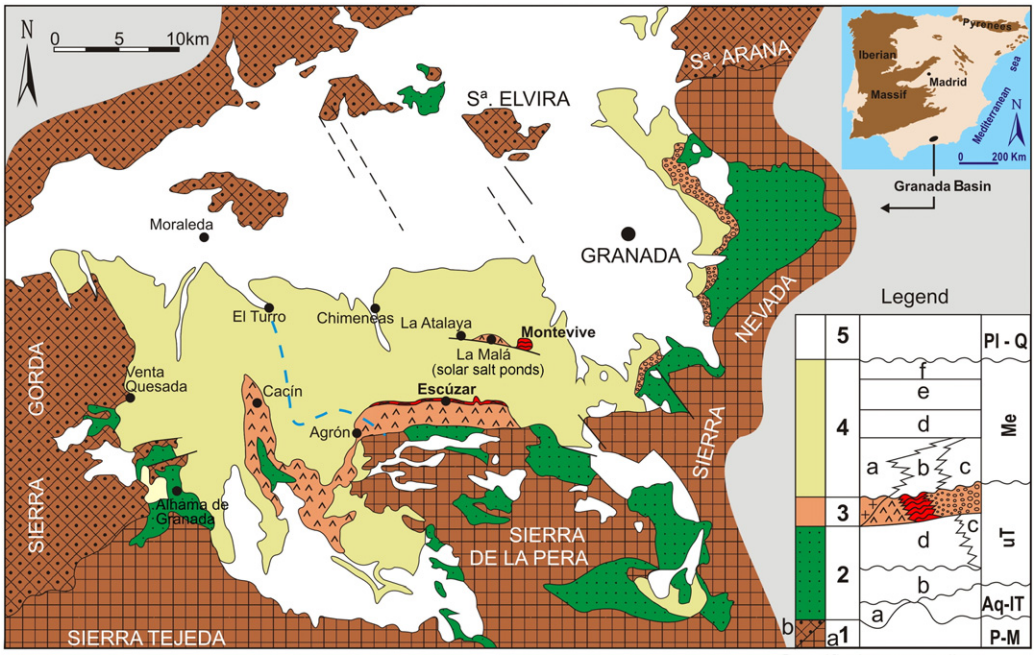

Fig. 1. Simplified geological map of the Granada Basin (modified after Martín et al., 1984, and after Dabrio et al., 1982).

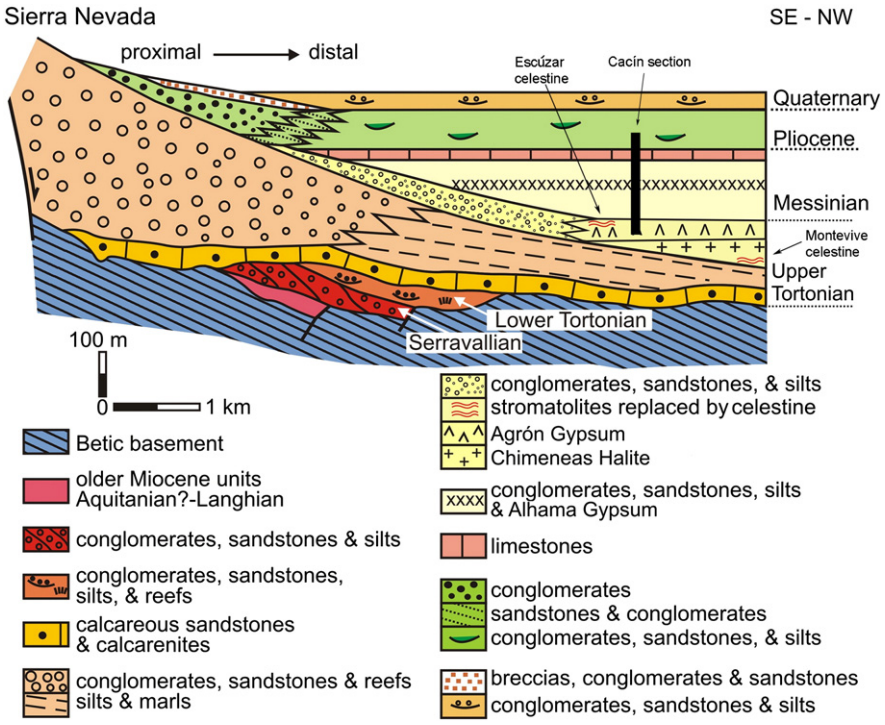

Fig. 2. Miocene to Pleistocene stratigraphy of the Granada Basin (after Braga et al., 1990).

Rodríguez-Fernández and Sanz de Galdeano, 2006) is formed, in ascending order, by the following units (Fig. 2): 1) Older Miocene units; 2) Serravallian–Lower Tortonian coastal and continental conglomerates and sandstones; 3) Tortonian (8.3–7.8 Ma) coastal and shallow marine calcarenites, calcareous sandstones and algal limestones; 4) Upper Tortonian (7.8–7.3 Ma) coastal, fan-delta conglomerates and patch-reefs grading basinward to open marine marls; 5) Late Tortonian (7.3–7.2 Ma) marine to continental evaporites (lower evaporites of Dabrio et al., 1982), mainly halite and gypsum; 6) Messinian siliciclastic lacustrine turbidites (La Malá turbidites) and evaporites (upper evaporites of Dabrio et al., 1982); and 7) Pliocene–Pleistocene continental deposits. A thick saline unit (up to 500 m) related to the Late Tortonian gypsum evaporites is found in the subsurface of the Granada Basin (García-Veigas et al., 2013).

Celestine outcrops are found in two parallel E–W belts, 5 km apart, located in the southern part of the Granada Basin (Martín et al., 1984; Ortega-Huertas et al., 1974; Sanz de Galdeano et al., 1976) (Fig. 1). The Montevive (Montevive Hill) and La Atalaya outcrops are situated in the northern belt, and the Escúzar orebody occurs in the southern one. Intense faulting now separates the outcrop belts which have been originally interpreted to belong to the same stratigraphic interval (Martín et al., 1984; Sanz de Galdeano et al., 1976).

The outcropping evaporite succession in the Granada Basin consists of two gypsum units separated by a clastic unit (Cacín Lutite; La Malá Turbidites) (Dabrio et al., 1982). In order to avoid confusion with the terminology used for the Mediterranean evaporites of the Messinian Salinity Crisis, we rename in the present article the lithostratigraphic units defined by Dabrio et al. (1982): Agrón Gypsum instead of *évaporites inférieures* (lower evaporites), and Alhama Gypsum instead of *évaporites supérieures* (upper evaporites). For the same purpose we shall denote as Chimeneas Halite the saline unit developed in the basin (García-Veigas et al., 2013).

3. Material and methods

A continuous section (Cacín section) that includes the three lithostratigraphic units (Agrón Gypsum, Cacín Lutite, and Alhama Gypsum) crops out along the road between Cacín and Alhama de Granada villages (Fig. 1). Partial sections can be observed in several outcrops and gypsum quarries in the southwestern and northeastern parts of the Granada Basin.

Celestine samples were collected in quarries of the Montevive and the Escúzar deposits. Limited exposure of mine workings, intense fracturing, and collapse breccias prevented precise stratigraphic control of the celestine sampling. The Cacín section of the evaporite sequence was sampled to study the primary gypsum, even though the lower part of the succession, in contact with the underlying marls, is missing. Additional gypsum samples were collected at different sites (Table 1, Fig. 1). A water sample was collected from a water-pumping well source which feeds a solar pond for halite production in La Malá village, very close to the Montevive deposit (Fig. 1).

Rock samples (celestine and gypsum) were cut with a diamond wire saw and then polished for mineral identification under an environmental scanning electron microscope (ESEM FEI-Quanta 2000) coupled with a backscattered electron detector (BSED) and an X-ray energy dispersive spectrometer (EDS EDAX Genesis). Thin sections of selected samples were made for optical observation with a polarizing microscope.

Sulfate isotope compositions ($\delta^{34}S_{V\text{-}CDT}$ and $\delta^{18}O_{V\text{-}SMOW}$) were obtained from gypsum and celestine samples dissolved in distilled water, boiled, acidified at pH ~ 3 and precipitated as barite by adding a $BaCl_2$ solution. The sulfur and oxygen isotope compositions were determined with a Carlo Erba 1108 Elemental Analyzer and a TC-EA unit respectively, both coupled to an IRMS Thermo Finnigan Delta Plus XP Spectrometer. The analytical error (2σ) was ±0.2‰ for $\delta^{34}S$ and ±0.4‰ for $\delta^{18}O$. Values obtained for the international standard NBS-127 were $\delta^{34}S$: 20.3 ± 0.1‰, and $\delta^{18}O$: 9.3 ± 0.2‰.

Strontium isotope ratios ($^{87}Sr/^{86}Sr$) were determined in 25 mg of powdered celestine and gypsum dissolved in 2 mL of distilled water preventing dissolution of carbonates and leaching of Sr from clay minerals. Samples were centrifuged and the supernatant removed taking care not to disturb any undissolved residue. The supernatant was dried, redissolved in HNO_3, and loaded onto Sr-Spec resin packed columns. The eluted Sr was loaded onto a single Ta filament with water and H_3PO_4, and oxidized in air. The isotope ratios were measured

Table 1
Isotope ($\delta^{34}S$, $\delta^{18}O$ and $^{87}Sr/^{86}Sr$) data of gypsum, halite and celestine samples of the Upper Miocene Granada Basin.

Location	Mineralogy/lithology/facies	Sample	$\delta^{34}S_{VCDT}$‰	$\delta^{18}O_{VSMOW}$‰	$^{87}Sr/^{86}Sr$
Alhama Gypsum					
Cacín	Microselenite	CN-33s	17.0	18.2	0.708442
Cacín	Gypsarenite	CN-33g	16.8	19.6	0.708425
Cacín	Fine-grained gypsum	CN-33b	17.2	18.2	0.708422
Cacín	Microselenite	CN-30	16.0	17.1	0.708458
Cacín	Gypsarenite	CN-28	15.9	15.7	0.708437
Cacín–Ventas de Huelma	Alabastrine secondary gypsum	CN-37	16.6	17.9	
Venta Quesada	Microselenite	VQ-1	15.8	16.1	0.708474
La Atalaya	Alabastrine secondary gypsum	AT-2	15.9	17.3	
Cacín Lutite					
Cacín	Selenite	CN-23	15.9	15.7	0.708571
Cacín	Fine-grained gypsum	CN-22	16.0	16.6	0.708554
Cacín	Selenite	CN-18	17.4	17.1	0.708714
Cacín	Selenite	CN-14	18.6	16.2	0.708777
La Malá	Alabastrine secondary gypsum	LM-1	16.4	16.8	0.708608
Agrón Gypsum					
Cacín	Fine-grained gypsum	CN-12	17.5	16.6	0.708711
Cacín	Selenite	CN-11	16.5	16.8	0.708695
Cacín	Selenite	CN-8	16.8	17.0	0.708738
Cacín	Selenite	CN-6s	17.1	17.9	0.708754
Cacín	Fine-grained gypsum	CN-6b	17.5	17.1	0.708716
Cacín	Selenite	CN-3	16.9	15.3	0.708763
Cacín	Selenite	CN-2	16.8	15.2	0.708782
Cacín	Selenite	CAC-2	17.4		0.708763
Cacín	Selenite	CAC-4	16.9		0.708758
Cacín	Selenite	CAC-6	16.7		0.708761
Agrón	Alabastrine secondary gypsum	AG-1	18.0		0.708676
La Atalaya	Alabastrine secondary gypsum	AT-1	17.4	16.5	
Montevive	Alabastrine secondary gypsum	MTV-14	16.4	16.2	0.708770
Escúzar	Alabastrine secondary gypsum	ME-6	18.3		0.708645
Escúzar	Alabastrine secondary gypsum	ME-7	17.8		0.708612
Escúzar	Alabastrine secondary gypsum	ESC-14	16.6	17.1	0.708663
Escúzar	Alabastrine secondary gypsum	ESC-15	16.7	16.4	0.708642
Montevive celestine deposit					
Montevive	Celestine	MTV-3	18.4	18.6	0.708813
Montevive	Celestine	MTV-5	18.7	18.1	0.708768
Montevive	Estroncianite	CE-1			0.708871
Montevive	Celestine	CE-2	17.8		0.708902
Montevive	Celestine	CE-3	21.3	15.7	0.708935
Montevive	Celestine	CE-4	19.6	15.7	0.708804
Montevive	Celestine	CE-5	20.4	18.0	0.708846
Escúzar celestine deposit					
Escúzar	Celestine	ESC-1	18.1	17.8	0.708593
Escúzar	Celestine	ESC-2	18.0	17.0	0.708641
Escúzar	Celestine	ESC-11	18.3	17.3	0.708657
Escúzar	Celestine	ESC-13	18.2	16.9	0.708660

on a VG 354 Mass-Spectrometer with precision of ±0.000014. The values obtained for international standard NBS-987 was 0.710288 ± 0.000014. Strontium isotope ratios were normalized to $^{87}Sr/^{86}Sr$: 0.1194.

Concentrations of cations in groundwater samples collected from the pumping well source were determined by ICP-MS, alkalinity (expressed as HCO_3^-) by titration and major anions (Cl^- and SO_4^{2-}) by liquid chromatography (HPLC).

4. Results

4.1. Gypsum: facies and petrology

The Agrón Gypsum in the Cacín section has a thickness of 40 m and consists of cm- to dm-thick beds of vertically-oriented, untwinned, primary selenite gypsum crystals (Fig. 3A) alternating with cm-thick layers of fine-grained (μm-sized) gypsum crystals commonly distorted by the growth of the larger selenite crystals (Fig. 3B). Marl interbeds, cm- to dm-thick, commonly occur at the base of the fine-grained gypsum intervals (Dabrio et al., 1982). Intercalated carbonate beds are rare but locally important in the upper part of the Escúzar area (Martín et al., 1984; Sanz de Galdeano et al., 1976).

In the studied section, the Cacín Lutite Unit is 140 m thick. Gypsum beds intercalated between lutites show lithofacies and textures (selenite and fine-grained gypsum) similar to those of the underlying Agrón Gypsum. According to Dabrio et al. (1982), a regional unconformity exists at the base of this unit which results in large thickness variations. In the La Malá section, the Cacín Lutite consists of over 100 m of siliciclastic lacustrine turbidites intercalated within lutite intervals ('La Malá Turbidites' of Dabrio et al., 1972, 1982).

The Alhama Gypsum, in the Cacín section, consists of 35 m of dm-thick beds of sand-sized primary gypsum crystals scattered in a muddy matrix (gypsarenites) (Fig. 3C). Vertically oriented gypsum crystals, with untwinned, bladed habits, up to 5 cm long (gypsum grass or microselenites) commonly occur at the base of the sandy-gypsum layers.

Primary gypsum lithofacies (selenites, microselenites, gypsarenites and fine-grained laminated gypsum) occur only in the southwestern part of the basin. In the rest of the basin all primary gypsum has been

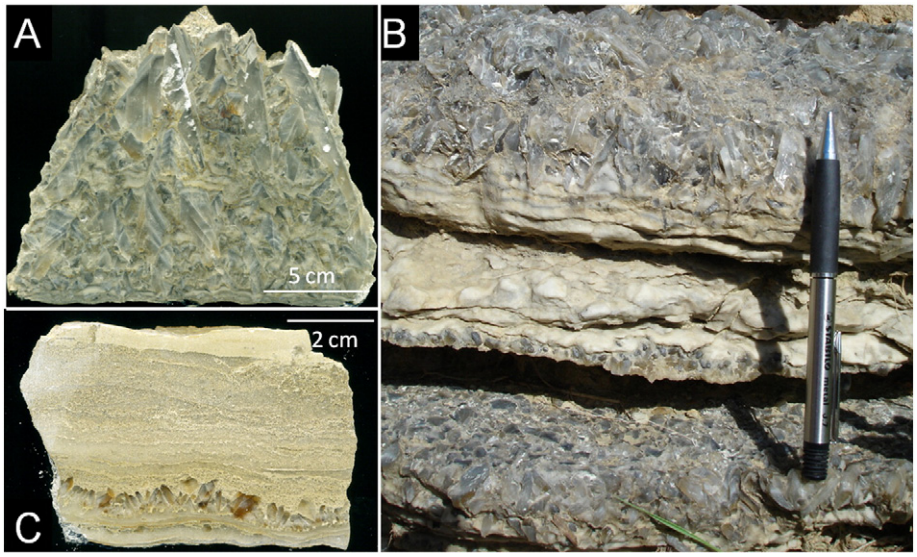

Fig. 3. Lithofacies of gypsum in the Granada Basin. A and B: Vertically-oriented selenite crystals with intercalations of fine-grained laminated gypsum (Agrón Gypsum, Upper Tortonian, Cacín section) (length of the pen 13 cm); C: Gypsarenite bed with vertically-oriented microselenites at the base (Alhama Gypsum, Messinian, Cacín section).

transformed into secondary gypsum (Dabrio and Martín, 1981), which consists of alabastrine nodules that preserve pseudomorphs of primary selenites containing anhydrite inclusions under the microscope. A line between the Agrón and El Turro sites can be drawn on the map (Fig. 1) separating a western area where primary gypsum predominates and an eastern area where secondary gypsum predominates.

Under the microscope, the primary gypsum samples reveal the presence of dolomicritic components showing rounded sections, circular (with a diameter of up to 100 μm) to elliptical, and with elongated sections up to 1 mm long (Fig. 4). These dolomicrite components are similar to those (shoestring or spaghetti-like) described by Vai and Ricci-Lucchi (1977) in the Messinian of Northern Apennines.

4.2. Celestine occurrences

The Montevive deposit (Fig. 5A), 90 m thick and 1.5 km^2 in area, occupies a hill close to La Malá village (Fig. 1). The hill is an antiformal structure (Martín and Ortega-Huertas, 1986) crossed by the main system of NW–SE normal faults related to the Padul–Nigüelas Fracture Zone and other conjugate fault systems active from the Upper Miocene to the present (Alfaro et al., 2001; Doblas et al., 1997; Fernández-Rubio et al., 1975). The hill mainly consists of celestine rock with $SrSO_4$ concentrations above 70%. Celestine occurs in roughly stratified beds, up to 50 cm thick. Single ore beds are difficult to trace laterally because of intense faulting, karstification and brecciation.

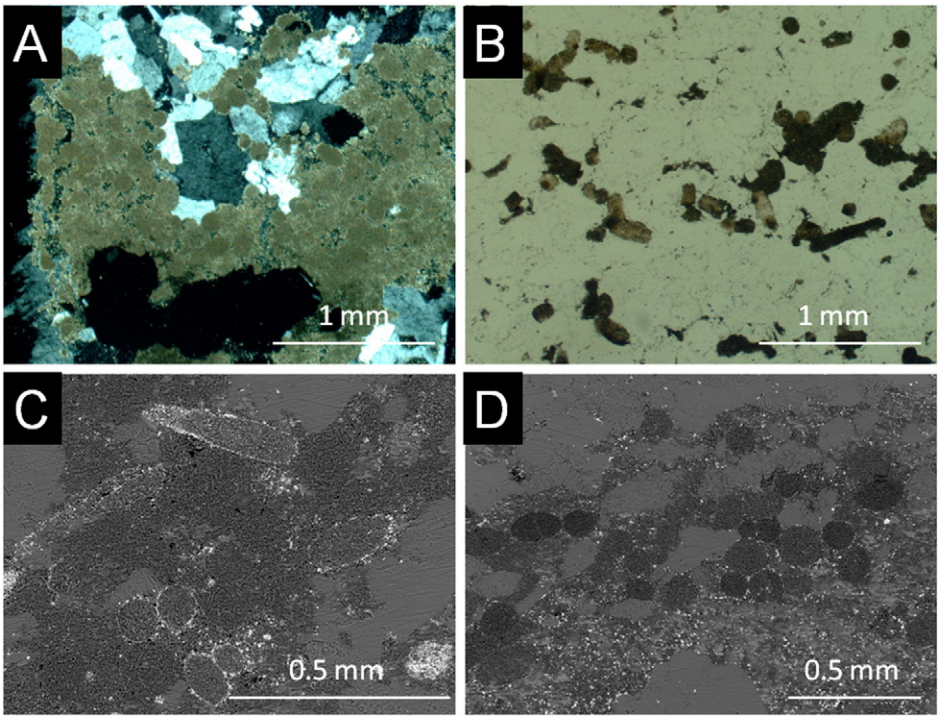

Fig. 4. Carbonate (dolomicrite) peloids in gypsum beds. A: Irregular carbonate layer containing peloids within a gypsarenite bed (photomicrograph with crossed Nicols); B: Carbonate peloids (dark colored) scattered between gypsum crystals (light colored) (photomicrograph with normal light); C and D: Carbonate peloids in gypsum beds (backscattered electron images). Celestine microcrystals (light colored) outline peloids in a fine-grained gypsum bed (C) and are scattered in mud in a gypsarenite bed (D).

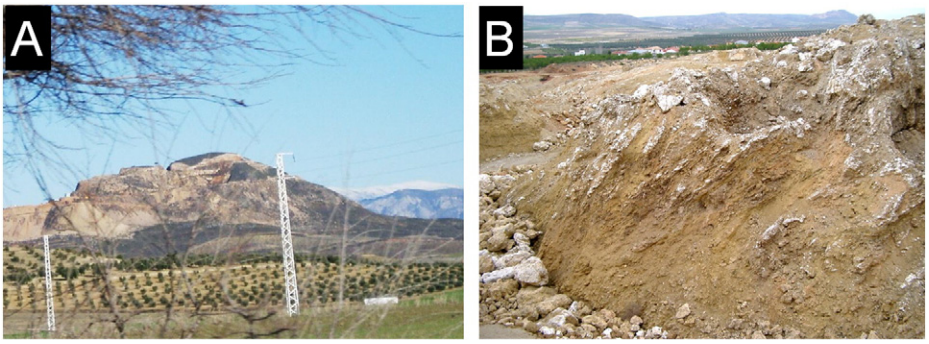

Fig. 5. Celestine ore deposits. A: General view of the Montevive Hill; B: Celestine quarry in the Escúzar deposit. Brownish celestine ore beds intercalate with white nodular gypsum beds.

The Escúzar deposit extends in an E–W belt, 10 km long and about 20–30 m thick, on top of and marginal to the gypsum deposits of the Agrón Gypsum (Martín and Ortega-Huertas, 1986). In contrast to Montevive, ore beds in Escúzar, up to 1 m thick, occur intercalated between meter thick intervals of alabastrine secondary gypsum. The Escúzar succession as a whole is highly tectonized (Fig. 5B). The average celestine content is lower than in the Montevive deposit, with values around 50%.

Mineralized beds in the two ore deposits are gray-brown to reddish in color, stained by secondary iron oxides. Celestine beds show a finely laminated stromatolite-like texture (Fig. 6A and B). Lamination is commonly disrupted and collapsed with tepees, mud-cracks and planar solution cavities. Celestine also fills molds of vertically-oriented, cm-sized precursor gypsum crystals (Fig. 6C). Breccias composed of laminated celestine clasts are commonly cemented by coarse crystalline celestine (Fig. 6D).

In the Montevive deposit, two parts can be clearly distinguished in some of the ore beds: a lower part laminated lithofacies and an upper part where cm-sized pseudomorphs after precursor selenite gypsum crystals occur; they are fully or partially replaced by celestine (Fig. 6C) and surrounded by fine-grained laminated matrix.

Under the microscope, the laminated lower part is made up of celestine alternating with thin dolomicrite laminae. Celestine replaces precursor μm-sized gypsum crystals which are outlined by micritic carbonate and thus can be recognized as pseudomorphs. The size of these replaced gypsum crystals increases toward the upper part of the bed which contains the larger cm-sized pseudomorphs of the selenite crystals. The micritic laminae show micropeloidal textures. The diameter of the dolomicritic micropeloids ranges from 20 to 40 μm (Fig. 7A) suggesting that they originated as microbial biofilms (Rouchy and Monty, 2000; Riding, 2000; Dupraz et al., 2009). Moreover, sections of larger (80–100 μm) and distinctly rounded dolomicritic peloids (with a maximum length of about 1 mm), surrounded by celestine, are also present (Fig. 7B and C); these components are similar to those already described in the gypsum units, and their origin will be discussed later.

Although celestine mainly replaces precursor primary gypsum crystals, carbonate micrite is also locally replaced by celestine laths. In the selenite gypsum pseudomorphs, a first generation of celestine crystals up to 1 mm long can be distinguished (Fig. 7D), growing inward from the external boundaries of the precursor crystal faces whereas a later generation of sparite calcite (up to 2 mm), locally associated with strontianite, fully or partially fills the empty cores of the pseudomorphs.

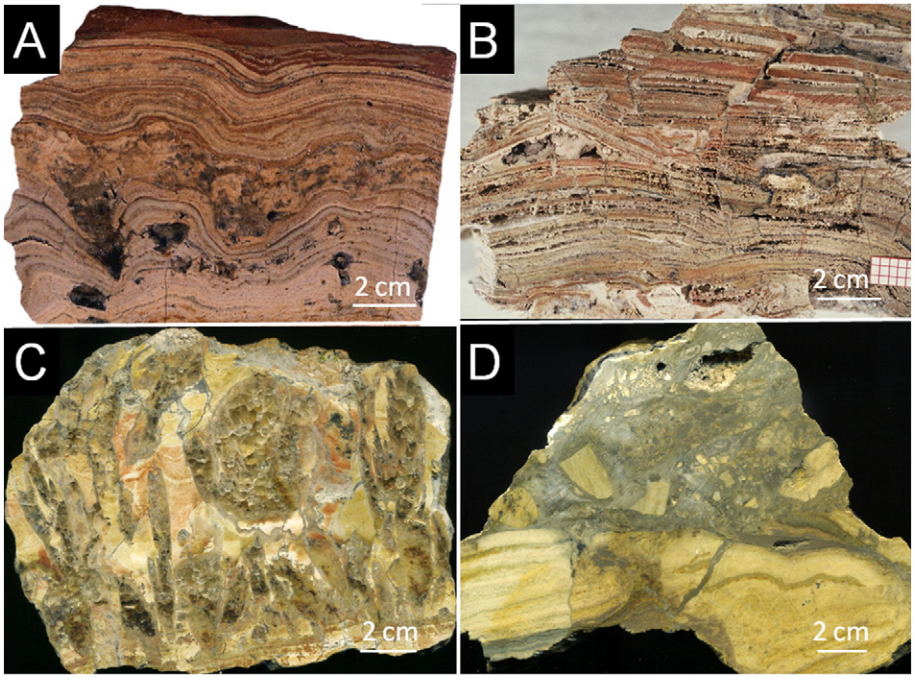

Fig. 6. Celestine ore facies. A and B: Laminated, stromatolite-like facies; C: Laminated celestine ore with vertically-oriented selenite gypsum pseudomorphs formed by coarse-crystalline celestine and calcite; D: Celestine ore breccia with laminated celestine ore clasts and mud pebbles.

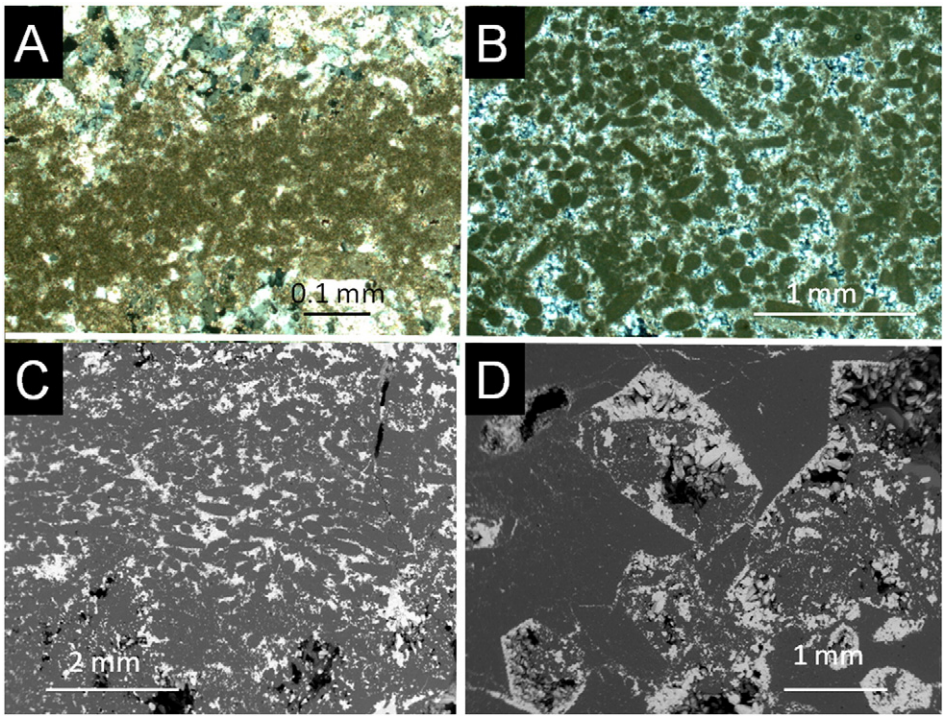

Fig. 7. Carbonate peloids in celestine ore. A: Carbonate lamina with micropeloidal texture between two laminae mainly made up of celestine microcrystals (photomicrograph with crossed polars); B and C: Fine-grained celestine associated with carbonate peloids (B: photomicrograph with crossed polars, C: backscattered electron image); D: Gypsum pseudomorphs formed by prismatic celestine in a carbonate mud bed (backscattered electron image).

In the Escúzar deposit carbonate components consist of medium- to coarse-crystalline calcite filling filaments similar in size and shape to those identified in Montevive. We interpret these calcite filaments as pseudomorphs via dolomicrite dissolution and calcite cementation of the moldic porosity.

4.3. Sulfate isotopes

Sulfur and oxygen isotope compositions of primary and secondary (alabastrine) gypsum, and of celestine samples are listed in Table 1. Sulfate isotope profiles of the Cacín section are shown in Fig. 8.

Average $\delta^{34}S$ values of 17.1 ± 0.6‰ (Agrón Gypsum), 17.0 ± 1.3‰ (Cacín Lutite), and 16.4 ± 0.6‰ (Alhama Gypsum) are significantly lower than those expected for Upper Miocene marine evaporites (21–23‰; Paytan et al., 1998). Average $\delta^{18}O$ counterpart values of 16.5 ± 0.9‰ (Agrón Gypsum), 16.5 ± 0.5‰ (Cacín Lutite), and 17.5 ± 1.3‰ (Alhama Gypsum) are higher than those expected for Upper Miocene marine evaporites (12–15‰; Claypool et al., 1980; Cendón, 1999). Sulfate isotope values are similar to those previously reported for gypsum samples coming from the evaporite units under study (Rouchy and Pierre, 1979).

Celestine $\delta^{34}S$ values range from 21.3 to 18.0‰, with average values of 19.4 ± 1.3‰ in the Montevive deposit, and of 18.2 ± 0.1‰ in the

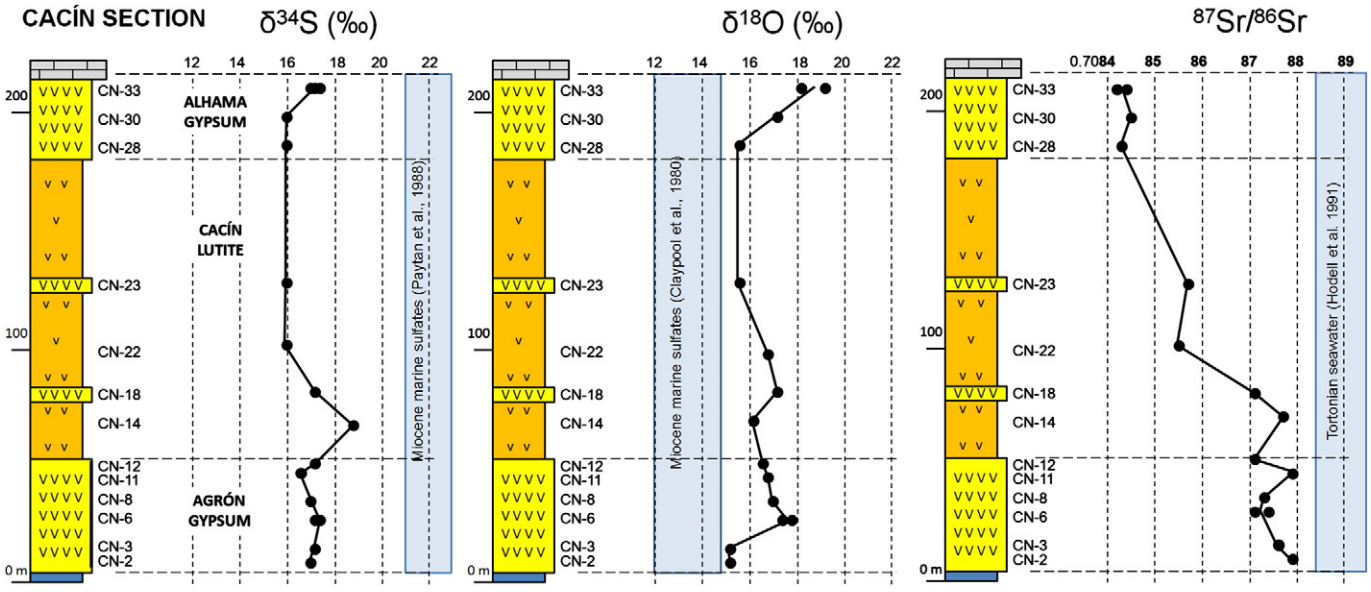

Fig. 8. Isotope profiles ($\delta^{34}S_{sulfate}$, $\delta^{18}O_{sulfate}$, and $^{87}Sr/^{86}Sr$) of the evaporite succession in the Cacín section (Granada, Spain).

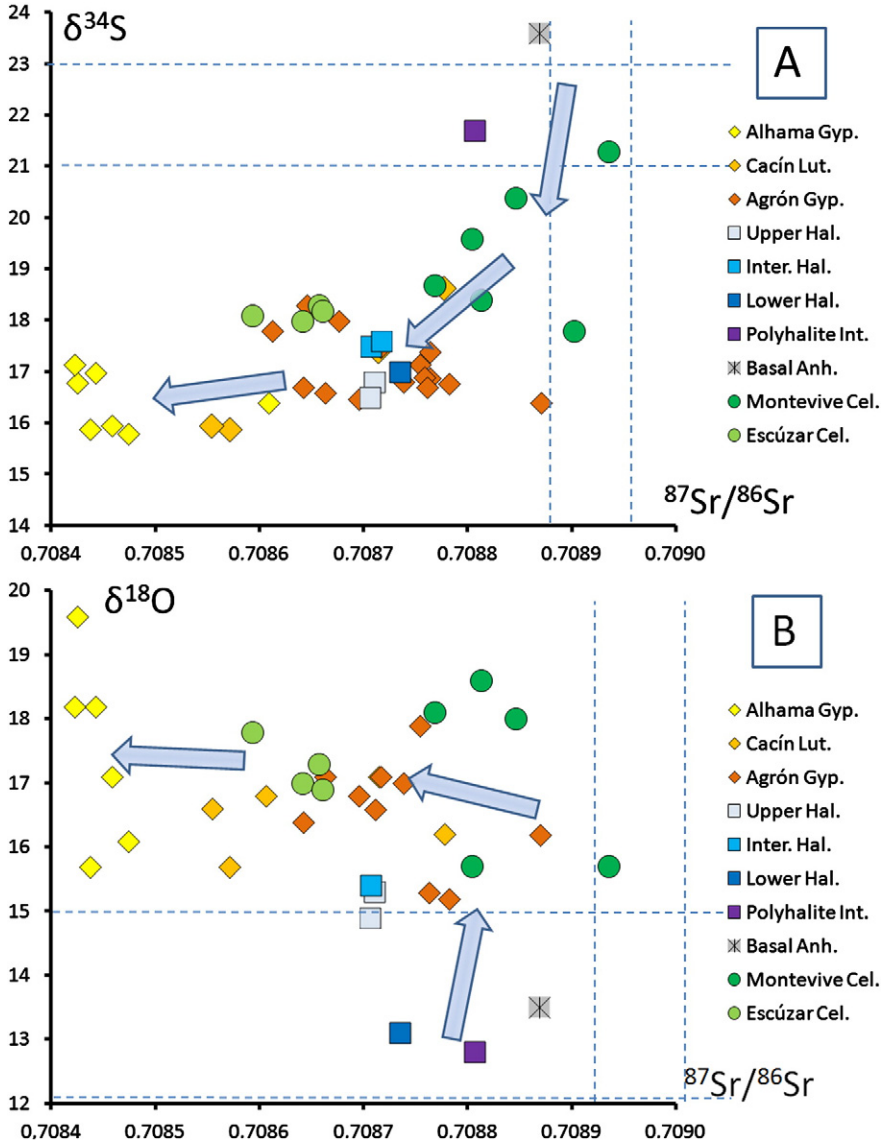

Fig. 9. Plots of isotope values (A: $\delta^{34}S_{sulfate}$ versus $^{87}Sr/^{86}Sr$, and B: $\delta^{18}O_{sulfate}$ versus $^{87}Sr/^{86}Sr$) of gypsum beds and celestine deposits in the Upper Tortonian–Messinian evaporite sequence of the Granada Basin. Isotope ratios from the saline unit (Lower, Intermediate and Upper Halite; García-Veigas et al., 2013) are also included. The dashed lines define the ranges that correspond to the Tortonian marine values.

Escúzar deposit. Sulfur isotope compositions of celestine samples in the Montevive deposit are always higher and have a wider range than in the Agrón Gypsum. However, $\delta^{34}S$ values in celestine samples of the Escúzar deposit are close to those in the Agrón Gypsum (Table 1).

Celestine $\delta^{18}O$ values range from 15.7 to 18.0‰ averaging 17.2 ± 1.4‰ in the Montevive deposit and 17.3 ± 0.4‰ in the Escúzar deposit. Oxygen isotope compositions of celestine in the two ore deposits are similar to those of the Agrón Gypsum.

4.4. Strontium isotopes

The strontium isotope profile for primary gypsum samples in the Cacín section shows an upward trend to less radiogenic ratios (Fig. 8). $^{87}Sr/^{86}Sr$ ratios are relatively homogeneous within each gypsum unit (Table 1) averaging 0.708716 ± 0.000054 in the Agrón Gypsum, and 0.708443 ± 0.000020 in the Alhama Gypsum. Intermediate values were found in the gypsum samples of the Cacín Lutite with a mean value of 0.708645 ± 0.000097. None of these values correspond to those expected for strontium in Tortonian seawater (~0.708900; Hodell et al., 1991).

Strontium isotope ratios for celestine differ in each deposit: 0.708848 ± 0.000059 in Montevive, and 0.708638 ± 0.000031 in Escúzar. Strontium isotope ratios of intercalated gypsum beds in the Escúzar deposit (0.708641 ± 0.000021) coincide with those of the corresponding ore samples (Fig. 9).

5. Discussion

Celestine in the Granada Basin was considered to have formed by early diagenetic replacement of freshwater stromatolitic carbonates accumulated in a coastal evaporitic environment; celestine mineralization was interpreted to have taken place in the mixing zones of coastal aquifers where stromatolitic carbonate interacted with subsurface fresh-water and SO_4^{2-}- and Sr^{2+}-rich, marine derived brines (Martín et al., 1984). Here we present an alternative mineralogenetic model based on new geochemical and petrologic data, and on more precise field observations integrating the ore deposits and the host evaporite succession.

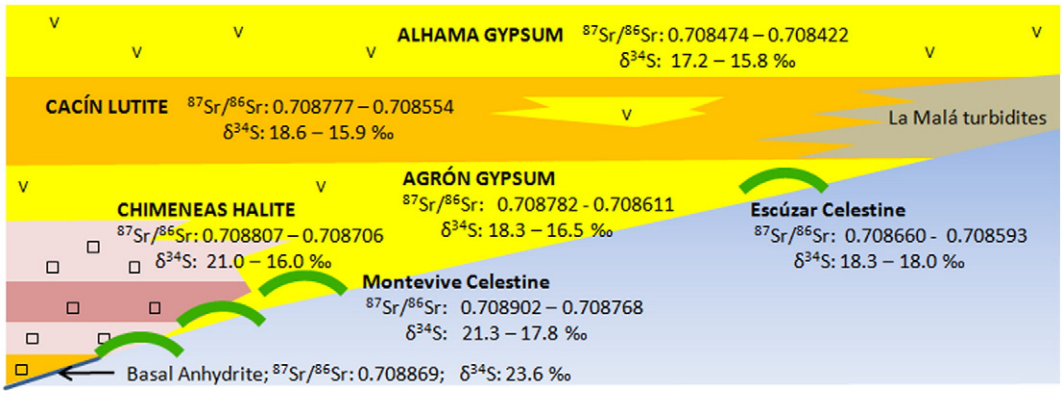

Fig. 10. Chemostratigraphic correlation chart of the Upper Miocene evaporite succession, including the celestine deposits, of the Granada Basin (Spain) based on isotope values ($^{87}Sr/^{86}Sr$ and $\delta^{34}S_{sulfate}$).

5.1. Gypsum evaporites (marine or nonmarine?)

The Agrón Gypsum (Figs. 1 and 2) conformably overlies marine basinal marls (Corbí et al., 2012; Martín et al., 1984). Although this unit was initially considered to be marine, no marine fauna has been reported in it. Abundant dm-thick gypsum beds made up of vertically oriented selenite crystals suggest a shallow evaporitic environment, but not necessarily marine.

Isotope data of the Agrón Gypsum ($\delta^{34}S$: ~17‰, $\delta^{18}O$: ~16‰; $^{87}Sr/^{86}Sr$: ~0.7087) indicate nonmarine water sources. These isotope values coincide with those reported for most of the underlying saline unit (García-Veigas et al., 2013). The Chimeneas Halite is underlain by a basal anhydrite bed, 20 cm thick. Geochemical data (fluid inclusion compositions in halite, and sulfur, oxygen and strontium isotopes in sulfate minerals) indicate that only the Basal Anhydrite and the lower part of the saline unit (Polyhalite Interval: polyhalite-bearing halite; García-Veigas et al., 2013) are marine in origin. As a whole, the Late Tortonian saline succession formed in a marine lagoon that evolved into a coastal salt-pan environment mainly fed by nonmarine water (García-Veigas et al., 2013).

Small mammal remains preserved in fluvial sediments interfingering with lacustrine sediments of the Cacín Lutite suggest an Early Messinian age for this continental interval (García-Alix et al., 2008). At that time, alluvial fan, fluvial, and lacustrine sediments were deposited in the basin. Evaporite conditions led to the accumulation of discrete gypsum beds in lakes. Sulfate isotope data of gypsum beds ($\delta^{34}S$: ~17‰, $\delta^{18}O$: ~16‰) are almost the same as those of the underlying Agrón Gypsum. However, strontium isotope ratios show intermediate values ($^{87}Sr/^{86}Sr$: ~0.7086) between the Agrón Gypsum and the Alhama Gypsum.

Evaporites of the Alhama Gypsum were originally interpreted as gypsum turbidites (Dabrio et al., 1982) and a clastic origin was assigned to the gypsarenites. The cm-sized gypsum crystals located at the base of the beds were thought to have formed as a result of recrystallization of the coarse-grained intervals of the turbidites (Dabrio and Martín, 1981). In the present work, we reinterpret the basal crystals as vertically-oriented, primary microselenites precipitated subaqueously on the lake floor. Microselenites in each bed were subsequently covered by clastic gypsarenite crystals suggesting a shallow environment. Isotope values of the Alhama Gypsum samples ($\delta^{34}S$: ~16‰, $\delta^{18}O$: ~18‰; $^{87}Sr/^{86}Sr$: ~0.7084) are much lower than those expected for Messinian marine evaporites.

With the exception of the lower part of the Chimeneas Halite (Basal Anhydrite and Polyhalite Interval; García-Veigas et al., 2013), the entire evaporite succession in the Granada Basin shows homogeneous sulfur isotope values ($\delta^{34}S$: ~17‰) suggesting a constant source of sulfate. However, $\delta^{18}O$ counterparts show a general trend to more positive values, from ~13‰ in the lower part of the Chimeneas Halite, to ~15‰ in the intermediate and upper parts of this saline succession, ~17‰ in the Agrón Gypsum and Cacín Lutite, and to ~18‰ in the Alhama Gypsum.

Sulfate isotope values of Upper Triassic (Keuper) evaporites ($\delta^{34}S$: ~14.4 ± 1.2‰, $\delta^{18}O$: ~12.2 ± 2.6‰; data in García-Veigas et al., 2013), which are widespread in the Betic Ranges and outcrop in the Moraleda and Sierra Elvira horsts in the northern part of the basin (Fig. 1), are significantly lower than those of the Granada Basin evaporites, suggesting that they are not the only sulfate source in the inflow waters that fed the basin. An additional sulfate source is required as formerly assumed by Rouchy and Pierre (1979) and Rouchy (1982).

The different sulfate isotope trends reported here (constant in $\delta^{34}S$ and increasing in $\delta^{18}O$) cannot be easily explained by common fractionation processes. Fractionation processes related to bacterial sulfate reduction (Kaplan and Rittenberg, 1964; Rees, 1973; Thode, 1991), or to recycling of older evaporites (Lloyd, 1968; Thode and Monster, 1965) affect both sulfur and oxygen isotopes. Preferential enrichment of $\delta^{18}O$ has been interpreted as the result of re-oxidation of reduced sulfur compounds (formed in organic-rich sediments) in oxygenated waters (Pierre, 1985). In any case, the sulfate isotope values of the entire gypsum succession, including the Agrón Gypsum, cannot be linked to strictly marine inflow waters.

5.2. Host rock in celestine deposits: carbonate or gypsum stromatolites?

Based on morphological aspects (mainly lamination) and on the abundance of peloidal textures and filaments, celestine in the Granada Basin was considered to have replaced carbonate stromatolites (Martín et al., 1984). However, the new insights provided in the present work have shown the significant contribution of gypsum to the original host rock. Thus, many of the laminated ore beds in the Montevive deposit reveal an original lithology made up, in the lower part, by alternating laminae of micrite and μm-sized gypsum crystals, and by selenitic gypsum crystals surrounded by micrite in the upper part. In both cases, carbonate has remained largely preserved whereas the gypsum crystals were completely replaced by celestine or dissolved and cemented by celestine and calcite.

As already stated, the micropeloidal textures making up the micrite laminae between the gypsum laminae in the Montevive ore beds, with grain diameters between 20 and 40 μm, are here interpreted as microbial biofilms. Microbial mats are abundant in modern evaporite environments dominated by gypsum precipitation but they rarely form lithified microbialites (Bąbel et al., 2011; Kobluk and Crawford, 1990; Oren et al., 1995; Ortí et al., 1984; Rouchy and Monty, 2000; Thomas, 1984). The role of microbes in gypsum precipitation has not been documented to date. However, recent papers dealing with this subject (Petrash et al.,

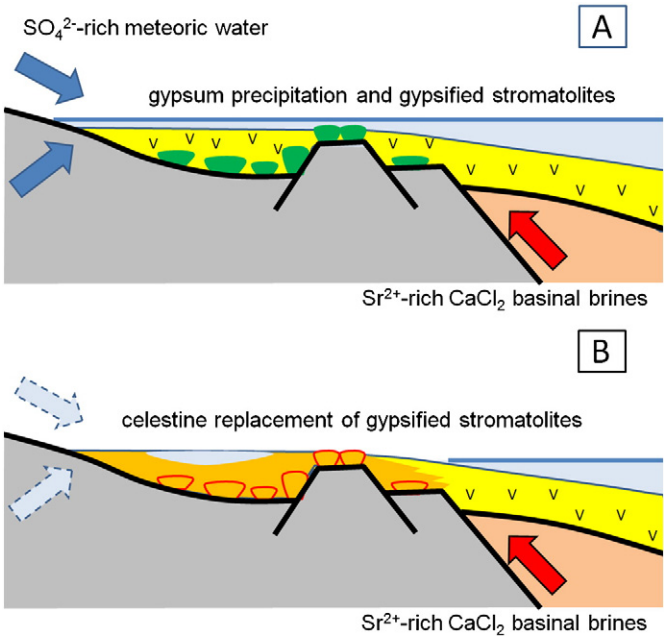

Fig. 11. Schematic drawing showing the model of early-diagenetic replacement of gypsified stromatolites by celestine. A: High-level stage with gypsum precipitation. Gypsified stromatolites proliferated locally along the basin margin, near thermal sources. B: Dry stage, during the decline of the SO_4^{2-}-rich meteoric input. The relative increase of $CaCl_2$ basinal brines in restricted coastal ponds promoted dissolution/replacement of previously formed gypsum by celestine.

2012; Vogel et al., 2010) provide evidence of biological influences on gypsum crystals textures and habits.

Stromatolites are considered to be a type of microbialite with laminated internal structure (Burne and Moore, 1987; Dupraz et al., 2009; Riding, 2000). *Microbialites* are defined as organosedimentary deposits formed as a result of benthic microbial community activity (Burne and Moore, 1987). The term *gypsum microbialite* has been used to designate the deposits formed by inorganic and passive precipitation of gypsum within the locus of benthic microbial communities (Bąbel et al., 2011). Rouchy and Monty (2000) believe the term *gypsified microbial deposit* is more appropriate in the case of gypsum deposits formed by the passive incorporation of microbial remains by mostly inorganic precipitation of gypsum.

In the case of the Montevive deposit, given that gypsum has been replaced or dissolved, specific interpretation of the microbial influence on its origin is not possible. However, field observations and petrographic study show that: 1) the host rock of the celestine ore was made up by gypsum and micritic carbonate displaying a finely laminated stromatolite-like structure, 2) the micritic laminae had a microbial origin, and 3) celestine mainly replaced gypsum. Thus, we reinterpret the host rock of the Montevive celestine ore as a gypsified stromatolite (sensu Rouchy and Monty, 2000).

The larger carbonate peloids (80–100 μm in diameter and with a maximum length of about 1 mm) found in the Montevive–Escúzar deposit, as well as in the Agrón, Cacín and Alhama gypsum beds are similar in shape and size to those described as spaghetti-like filaments in the Messinian gypsum of the northern Apennines by Vai and Ricci-Lucchi (1977) and identified in Messinian gypsum and carbonate deposits of Sicily, Ionian islands, Algeria, Crete and Cyprus (Rouchy and Monty, 2000). Similar peloidal grains have been assigned to: 1) fecal pellets of brine shrimp (Guido et al., 2007; Schreiber, 1978); 2) cyanobacteria: *Scytonema* (Rouchy and Monty, 1981) and *Geitlerinema* (Panieri et al., 2010); and 3) the sulfur bacteria *Beggiotoa* (Oliveri et al., 2010). Baltres and Medeşan (1978) described fecal pellets of *Artemia salina* from Techirghiol Lake (Romania) which display shapes (small rod-like bodies) and sizes very similar to those found in the evaporites of the Granada Basin. Moreover, brine shrimp fecal pellets in the Salar of Uyuni are also similar to those of the Montevive deposit (T.K. Lowenstein, personal communication). Considering that the size of these peloids is noticeably larger than any known from a single bacterial sheath or cell, the assignment to any specific microbial group is questionable. Considering all the above, we interpret these large peloids as brine shrimp fecal pellets that were trapped within gypsum crystals during growth.

5.3. Chemostratigraphy

In the absence of fossils or suitable volcanic rocks for radiometric dating, sulfate and strontium stable isotopes can be used for age assignments in marine evaporites. With the exception of the Basal Anhydrite and the lower part of the Chimeneas Halite (Polyhalite Interval), sulfate and strontium isotope values in the evaporite succession deviate from the Upper Miocene marine values. Variations in sulfate and strontium isotopes (Fig. 9) show marked trends suitable for stratigraphic correlations and for estimating the timing of formation of the celestine ore deposits.

Assuming that the celestine deposits were formed during early diagenesis, the strontium isotope ratios of the ore deposits should be similar to those of the host evaporites. Furthermore, if no significant fractionation occurred during gypsum dissolution and celestine precipitation, the sulfate isotope compositions of both the celestine ore and the host gypsum should also be similar. These requirements can only be checked in the Escúzar deposit where several gypsum beds are preserved between celestine ore beds. Strontium isotope ratios of celestine and gypsum beds in the Escúzar deposit are all close to 0.7086 whereas sulfur isotope compositions range between 16.6 and 18.3‰.

Based on isotope values, particularly $^{87}Sr/^{86}Sr$ ratios, the timing of formation of each ore deposit is proposed. In the Montevive deposit, strontium ratios of celestine show a wide range of values (~0.7089–0.7087) that fit those of the whole Chimeneas Halite succession (~0.7088–0.7087) (Fig. 9). Moreover, sulfur isotope compositions of celestine in the Montevive deposit (~18–21‰) show intermediate values between those obtained in the marine Polyhalite Interval (~21‰) and those corresponding to the rest of the saline unit (~18–16‰) (García-Veigas et al., 2013). Based on these data, we propose the stratigraphic correlation of the gypsified stromatolite in the Montevive deposit – and its celestine replacement – with the Chimeneas Halite unit (Fig. 10).

Strontium isotope ratios in the Escúzar celestine (~0.7086) match the values obtained at the top of the Agrón Gypsum and in the gypsum beds of the Cacín Lutite.

Chemostratigraphic correlations of the evaporite units and the celestine deposits based on Sr and S isotope data are shown in Fig. 10. The two ore deposits are interpreted to have formed by similar processes, but at different times, and from a source with different strontium isotope ratios.

5.4. Strontium source and celestine formation

Hanor (2004) proposed a model for celestine formation based on the contribution of Sr^{2+}-rich basinal brines interacting with SO_4^{2-}-rich surface waters or with Ca-sulfate deposits. This model applies reasonably well to the Montevive–Escúzar deposit.

Basinal brines (sensu Hanor, 1994), also called formation brines, occur in deep sedimentary basins as: 1) connate brines trapped during evaporitic events, 2) the product of dissolution of halite-bearing evaporites at depth, and 3) the product of diagenetic processes (dolomitization, albitization, bacterial sulfate reduction, etc.). $CaCl_2$ diagenetic–hydrothermal waters are typically subsurface basinal brines, with low contents of SO_4^{2-} and HCO_3^-. Ca^{2+} enrichment in such brines occurs by rock/sediment–water diagenetic interactions at

Table 2
Chemical composition (mol/L) of well water feeding solar salt-ponds of La Malá (Granada, Spain), and comparison with seawater compositions during evaporation.

	Cl^-	HCO_3^-	SO_4^{2-}	Na^+	Ca^{2+}	Mg^{2+}	K^+	Sr^{2+}
La Malá brine	3.926	0.006	0.031	3.364	0.040	0.032	0.005	0.000388
Seawater	0.551	0.004	0.028	0.470	0.010	0.053	0.010	0.000087
Seawater at the beginning of gypsum precipitation	1.729		0.092	1.643	0.038	0.186	0.037	0.000342
Seawater at the beginning of halite precipitation	4.463		0.173	4.478	0.005	0.518	0.100	0.000285

depth at elevated temperatures. These brines may discharge as springs and seeps in closed basins driven by thermal anomalies related to volcanism and faulting (Lowenstein and Risacher, 2009).

The Cenozoic is characterized by SO_4^{2-}-rich ($SO_4^{2-} > Ca^{2+}$) seawater (Brennan et al., 2013; Horita et al., 2002; Lowenstein et al., 2001). Assuming a Sr^{2+} concentration in Miocene seawater similar to current values (~8 ppm; Bernat et al., 1972), the high sulfate concentration produced during evaporation of seawater prevents the enrichment of Sr^{2+} in SO_4^{2-}-rich marine-derived brines due to the low solubility of strontium sulfate. Average strontium concentration in modern freshwater is <1 ppm. Meteoric waters evolve during evaporative concentration in closed basins to alkaline or sulfate-rich brines. In such brines, given the low solubility of strontium sulfates and carbonates, Sr^{2+} becomes exhausted early on, trapped in disseminated celestine and minor strontianite. In the absence of volcanic rocks, biogenic carbonate sediments are by far the most important Sr reservoir (Capo et al., 1998). Diagenetic recrystallization of carbonate sediments, mainly biogenic aragonite, releases strontium (Baker and Bloomer, 1988; Elderfield and Gieskes, 1982), which may be stored in sulfate-poor and Cl-rich basinal waters as a result of the high solubility of $SrCl_2$ (538 g/L). Hence, Sr^{2+}-enriched basinal waters may form by: 1) evaporative concentration of SO_4^{2-}-depleted seawater, 2) evaporative concentration of sulfate-poor meteoric water, and 3) influx of $CaCl_2$ diagenetic–hydrothermal brines (Lowenstein and Risacher, 2009).

As discussed above, gypsum deposits in the Granada Basin, where stratabound celestine deposits now occur, formed from nonmarine waters, or from mixing of a small proportion of residual marine water with meteoric water. Moreover, sulfate-poor meteoric waters seem unrealistic taking into account the thickness of the gypsum deposits accumulated in the basin. Thus, an additional source of strontium is required to produce the large celestine deposits. We suggest that basinal brines, ascending as diagenetic–hydrothermal waters, could be the main Sr^{2+} source.

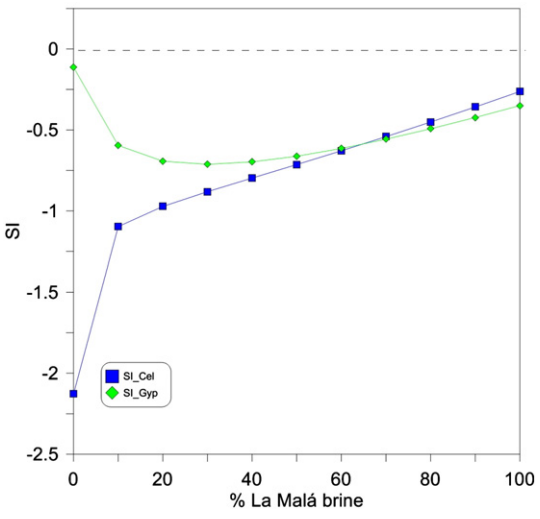

Fig. 12. Saturation index for celestine, gypsum and halite calculated for mixed volumes of freshwater saturated in gypsum with increasing proportions of present-day La Malá brine.

The marine strontium isotope curve displays a trend to more radiogenic ratios during the Neogene (Burke et al., 1982; McArthur et al., 2001; Veizer et al., 1999). The infilling of the Granada Basin, prior to its final continentalization, spans from Early Miocene ($^{87}Sr/^{86}Sr$: ~0.7082–0.7086) to Late Tortonian ($^{87}Sr/^{86}Sr$: ~0.7089–0.7090). Strontium ratios at the base of the Chimeneas Halite (~0.7088 in the Basal Anhydrite) match those expected for Late Tortonian seawater but decrease progressively through the saline unit (~0.7088–0.7087) (García-Veigas et al., 2013), the Agrón Gypsum (~0.7088–0.7086) and the Cacín Lutite (~0.7087–0.7085) to ~0.7084 in the Alhama Gypsum.

Sr^{2+} enrichments and $^{87}Sr/^{86}Sr$ decreasing trends have been reported in interstitial waters collected from modern marine sediments (Elderfield and Gieskes, 1982). These trends may be explained by: 1) alteration of volcanic materials ($^{87}Sr/^{86}Sr$: 0.7027–0.7050), 2) hydrothermal activity in regions of young oceanic crust and intrusive rocks ($^{87}Sr/^{86}Sr$: ~0.7050), and 3) diagenetic recrystallization of carbonates. In the absence of volcanic rocks and oceanic crust in the Granada Basin, the decreasing trend in $^{87}Sr/^{86}Sr$ requires isotopic equilibrium of basinal brines with older carbonate sediments by means of diagenetic reactions as the residence time increases.

Strontium isotope ratios in the upper part of the evaporitic succession (Alhama Gypsum; ~0.7084) fit well with values expected for the oldest marine sediments filling the Granada Basin (Early–Middle Miocene). However, these sediments are not volumetrically sufficient to have been the source of the large quantities of Sr^{2+} required for ore deposits. Therefore, other mechanisms, such as interbasin flow (Belcher et al., 2009) of diagenetic–hydrothermal waters must be considered.

The scenario envisaged for celestine formation begins with deposition of the Agrón Gypsum in a lacustrine environment fed by $CaSO_4$-rich meteoric water. Homogeneous sulfur isotope values ($\delta^{34}S$ ~ 17‰) suggest recycling of older Mesozoic evaporites. As indicated by fluid inclusion compositions in the Chimeneas Halite (García-Veigas et al., 2013), an additional source of $CaCl_2$-rich (Sr^{2+}-rich) hydrothermal water is needed. Gypsum precipitation took place at the basin margins while halite deposits formed in the basin center during hypersaline episodes of the lake. During dry periods, meteoric inflow declined and the lake was mainly fed by $CaCl_2$ diagenetic–hydrothermal brines rising through subsurface fractures (Fig. 11). At times, these lacustrine settings evolved into marginal ponds fed by $CaCl_2$ groundwater. The low sulfate contents ($Ca^{2+} > SO_4^{2-}$) of these diagenetic–hydrothermal waters stimulated dissolution, karstification and generation of collapse breccias in the previously formed gypsified stromatolites. Combination of high Sr^{2+} concentrations in $CaCl_2$ waters and the increase in the sulfate concentration by means of dissolution of gypsified stromatolites led to celestine precipitation, replacement of gypsum, and filling of the open spaces by celestine.

Modern thermal springs related to faults are widespread in the Granada Basin and other Neogene Betic basins (Cerón et al., 1998, 2000; López-Chicano and Pulido-Bosch, 1995; López-Chicano et al., 2001). In La Malá village (Fig. 1), close to the Montevive Hill, a saline stream (Arroyo del Salado) flows close to a thermal spring (Baños de La Malá) and nearby solar salt ponds. The water collected from the well feeding the ponds (Table 2) is a Ca^{2+}-rich brine with Sr^{2+} concentrations (30 ppm) higher than those in evaporated seawater. This type of brine is not derived from dissolution of halite by deep waters because those brines would not be enriched in Ca^{2+} and Sr^{2+}.

In order to evaluate the validity of the proposed model we mixed varying proportions of La Malá water (as an example of basinal brine) with freshwater saturated in $CaSO_4 \cdot 2H_2O$ (2.4 g/L) simulating meteoric dissolution of exposed gypsum. Celestine saturation was calculated with the PHREEQC (version 3-0-6) software using Pitzer activity coefficients for concentrated brines (Parkhurst and Appelo, 1999, 2005). In all cases gypsum precipitation did not occur due to the low sulfate concentration in La Malá brine (Fig. 12). Beyond a mixing ratio of 60% of La Malá brine, saturation indexes of celestine became higher than those of gypsum, suggesting that this type of brine may be responsible for the celestine mineralization.

This proposed model for the Montevive–Escúzar celestine deposits is supported by: 1) local distribution of stromatolites and celestine mineralization in areas affected by intense tectonic activity since the Upper Miocene (Fernández-Rubio et al., 1975); 2) thermal activity in the Montevive Hill such as the vent (the Fumarole Cave) that acts as a conduit for ascending hot waters. Modern hot springs are also located in La Malá (Fernández-Rubio et al., 1975); 3) evidence of gypsum dissolution: selenite molds, sedimentary breccias and karstification surfaces; 4) chemical composition (Sr^{2+}-rich, $Ca^{2+} > SO_4^{2-}$) of modern saline groundwaters feeding solar salt ponds in La Malá; and 5) fluid inclusion evidence of Ca^{2+}-rich (SO_4^{2-}-poor) inflow waters during Upper Tortonian halite precipitation (García-Veigas et al., 2013); and 6) sulfate and strontium isotope values of celestine and hosting evaporites.

6. Conclusions

The large celestine deposits of Montevive and Escúzar (Granada, Spain) are associated with the evaporite succession (gypsum/anhydrite and halite) of the Granada Basin (Upper Miocene) and particularly with the Agrón Gypsum. The isotopic composition of the sulfate of this gypsum unit indicates that it was mainly formed from nonmarine parent waters.

Celestine orebeds show stromatolitic lamination as indicated by micropeloidal textures in the preserved dolomicrite laminae, interpreted as microbial biofilms. Large dolomicrite peloids interpreted as fecal pellets of brine shrimps are preserved in celestine orebeds. Similar peloids are also present in the Agrón and Alhama gypsum beds,

Celestine replaces precursor gypsum laminae as revealed by abundant pseudomorphs of gypsum microcrystals; moreover, cm-sized selenite pseudomorphs can be also recognized in the celestine ore-beds. Thus, the precursor lithology of the celestine deposit is interpreted as gypsified stromatolites (sensu Rouchy and Monty, 2000).

Basinal brines, ascending as diagenetic–hydrothermal waters, are considered to have been the main Sr^{2+} source. This interpretation is supported by the intense faulting and modern thermal vents, hot springs and saline springs, with $CaCl_2$-rich, high Sr^{2+}, and low SO_4^{2-} compositions, that occur in the Montevive area. Gypsified stromatolites formed along the basin margin mainly from meteoric water enriched in $CaSO_4$ by recycling of older evaporites. Celestine formation is envisaged as an early-diagenetic process taking place at times of low water level caused by a decline in meteoric water inflow during dry periods. Gypsified stromatolites were then exposed to the $CaCl_2$ thermal waters which promoted gypsum dissolution. The released sulfate, combined with the dissolved strontium, triggered celestine precipitation and gypsum replacement.

Based on the strontium and sulfur isotope data of the Montevive and Escúzar deposits, it is proposed that they formed by similar mechanisms but at different times and from source waters with different strontium isotope ratios.

Acknowledgments

This study was supported by the projects CGL2009-11096 and CGL2010-20857 of the Spanish Government, and 2009-SGR1451 of the Catalan Government. The authors are indebted to Jordi Illa, Rosa Maria Marimon and Eva Aracil (Universitat de Barcelona) for their technical support, and to Enrique Sanz (Geomnia Natural Resources) for subsurface information data. Tim K. Lowenstein (Binghamton University) and Jean M. Rouchy (Muséum National d'Histoire Naturelle, Paris) are thanked for helpful suggestions on the early version of the manuscript. We also would like to thank B. Charlotte Schreiber for her very insightful review.

References

Alfaro, P., Galindo-Zaldívar, J., Jabaloy, A., López-Garrido, A.C., Sanz de Galdeano, C., 2001. Evidence for the activity and paleoseismicity of the Padul Fault (Betic Cordillera, southern Spain). Acta Geol. Hisp. 36, 283–295.

Bąbel, M., Olszewska-Nejbert, D., Bogucki, A., 2011. Gypsum microbialite domes shaped by brine currents from the Badenian evaporites of Western Ukraine. In: Reitner, J., Quéric, N.V., Arp, G. (Eds.), Advances in Stromatolite Geobiology Lecture Notes in Earth Sciences. 131. Springer-Verlag, Berlin Heidelberg, pp. 297–320.

Baker, P.A., Bloomer, S.H., 1988. The origin of celestite in deep-sea carbonate sediments. Geochim. Cosmochim. Acta 52, 335–339.

Baltres, A., Medeşan, A., 1978. High-magnesian calcite in fecal pellets of *Artemia salina* from Techirghiol Lake. Sediment. Geol. 20, 281–290.

Belcher, W.R., Bedinger, M.S., Back, J.T., Sweetkind, D.S., 2009. Interbasin flow in the Great Basin with special reference to the southern Funeral Mountains and the source of Furnace Creek springs, Death Valley, California, USA. J. Hydrol. 369, 30–43.

Bernat, M., Church, T., Allegre, C.J., 1972. Barium and strontium concentrations in Pacific and Mediterranean sea water profiles by direct isotope dilution mass spectrometry. Earth Planet. Sci. Lett. 16, 75–80.

Bernstein, R.E., Betzer, P.R., Feely, R.A., Byrne, R.H., Lamb, M.F., Michaels, A.F., 1987. Acantharia fluxes and strontium to chlorinity ratios in the North Pacific Ocean. Science 237, 1490–1494.

Braga, J.C., Martín, J.M., Alcalá, B., 1990. Coral reefs in coarse-terrigenous sedimentary environments (Upper Tortonian, Granada Basin, southern Spain). Sediment. Geol. 66, 135–150.

Braga, J.C., Martín, J.M., Quesada, C., 2003. Patterns and average rates of late Neogene–Recent uplift of the Betic Cordillera, SE Spain. Geomorphology 50, 3–26.

Braitsch, O., 1971. Salt Deposits: Their Origin and Composition. Springer-Verlag, New York (279 pp.).

Brennan, S.T., Lowenstein, T.K., Cendón, D.I., 2013. The major-ion composition of Cenozoic seawater: the past 36 million years from fluid inclusions in marine halite. Am. J. Sci. 313, 713–775.

Brodtkorb, M.A., Ramos, V., Barbieri, M., Ametrano, S., 1982. The evaporitic celestine–barite deposits of Neuqen, Argentina. Mineral. Deposita 17, 423–436.

Burke, W.H., Denison, R.E., Hetherington, E.A., Koepnick, R.B., Nelson, H.F., Otto, J.B., 1982. Variation of seawater $^{87}Sr/^{86}Sr$ throughout Phanerozoic time. Geology 10, 516–519.

Burne, R.V., Moore, L.S., 1987. Microbialites: organosedimentary deposits of benthic microbial communities. Palaios 2, 241–254.

Capo, R.C., Stewart, B.W., Chadwick, O.A., 1998. Strontium isotopes as tracers of ecosystems processes: theory and methods. Geoderma 82, 197–225.

Carlson, E.H., 1987. Celestite replacements of evaporites in the Salina Group. Sediment. Geol. 54, 93–112.

Cendón, D.I., 1999. Evolución geoquímica de cuencas evaporíticas Terciarias: implicaciones en la composición isotópica del sulfato disuelto en el océano durante el Terciario(Ph.D.) Universitat de Barcelona (270 pp., In Spanish, http://www.tdx.cat/handle/10803/81705).

Cerón, J.C., Pulido-Bosch, A., Sanz de Galdeano, C., 1998. Isotopic identification of CO_2 from a deep origin in thermomineral waters of southeastern Spain. Chem. Geol. 149, 251–258.

Cerón, J.C., Martín-Vallejo, M., García-Rossell, L., 2000. CO_2-rich thermomineral groundwater in the Betic Cordilleras, southeastern Spain: genesis and tectonic implications. Hydrogeol. J. 8, 209–217.

Claypool, G.E., Holser, W.T., Kaplan, I.R., Sakai, H., Zak, I., 1980. The age curves of sulfur and oxygen isotopes in marine sulfate and their mutual interpretation. Chem. Geol. 28, 199–260.

Corbí, H., Lancis, C., García-García, F., Pina, J.A., Soria, J.M., Tent-Manclús, J.E., Viseras, C., 2012. Updating the marine biostratigraphy of the Granada Basin (central Betic Cordillera). Insight for the Late Miocene paleogeographic evolution of the Atlantic–Mediterranean Seaway. Geobios 45, 249–263.

Dabrio, C.J., Martín, J.M., 1981. Yesos diagenéticos en la Depresión de Granada. Boletín de la Real Sociedad Española de Historia Natural. Sección Geología, 79, pp. 215–233 (in Spanish).

Dabrio, C.J., Carcía-Yebra, R., Gonzalez-Donoso, J.M., Vera, J.A., 1972. Turbiditas asociadas a evaporitas (Mioceno, La Malá, Depresión de Granada). Cuad. Geol. 3, 139–164 (in Spanish).

Dabrio, C.J., Martín, J.M., Megias, A.G., 1982. Signification sédimentaire des évaporites de la depression de Granade (Espagne). Bull. Soc. Geol. Fr. 4, 705–710 (in French).

Deckker, P., 2004. On the celestite-secreting *Acantharia* and their effect on seawater strontium to calcium ratios. Hydrobiologia 517, 1–13.

Dill, H.G., Henjes-Kunst, F., Berner, Z., Stüben, D., 2009. Miocene diagenetic and epigenetic strontium mineralization in calcareous series from Cyprus and the Arabian Gulf: metallogenetic perspective on sub- and suprasalt redox-controlled base metal deposits. J. Asian Earth Sci. 34, 557–576.

Doblas, M., Mahecha, V., Hoyos, M., López-Ruiz, J., 1997. Slickenside and fault surface kinematics indicators on active normal faults of the Alpine Betic Cordilleras, Granada, southern Spain. J. Struct. Geol. 19, 159–170.

Dupraz, C., Reid, R.P., Braissant, O., Decho, A.W., Norman, R.S., Visscher, P.T., 2009. Processes of carbonate precipitation in modern microbial mats. Earth Sci. Rev. 96, 141–162.

Elderfield, H., Gieskes, J.M., 1982. Sr isotopes in interstitial waters of marine sediments from Deep Sea Drilling Project cores. Nature 300, 493–497.

Fernández-Rubio, R., Eraso, A., Ortega-Huertas, M., Arana, R., Rojas, E., 1975. Estudio de la sima termal de Las Fumarolas (Montevives, Granada) *Cuadernos Geográficos de la Universidad de Granada*. 1, pp. 127–147 (in Spanish).

García-Alix, A., Minwer-Barakat, R., Martín, J.M., Martín-Suarez, E., Freudenthal, M., 2008. Biostratigraphy and sedimentary evolution of Late Miocene and Pliocene continental deposits of the Granada Basin (southern Spain). Lethaia 41, 431–446.

García-Veigas, J., Cendón, D.I., Rosell, L., Ortí, F., Torres Ruiz, J., Martín, J.M., Sanz, E., 2013. Salt deposition and brine evolution in the Granada Basin (Late Tortonian, SE Spain). Palaeogeogr. Palaeoclimatol. Palaeoecol. 369, 452–465.

González-Sánchez, F., Camprubí, A., González-Partida, E., Puente-Solís, R., Canet, C., Centeno-García, E., Atudorei, V., 2009. Regional stratigraphy and distribution of epigenetic stratabound celestine, fluorite, barite and Pb–Zn deposits in the MVT province of northeastern Mexico. Mineral. Deposita 44, 343–361.

Guido, A., Jacob, J., Gautret, P., Laggoun-Défarge, F., Mastandrea, A., Russo, F., 2007. Molecular fossils and other organic markers as paleoenvironmental indicators of the Messinian Calcare di Base Formation: normal versus stressed marine deposition (Rossano Basin, northern Calabria, Italy). Palaeogeogr. Palaeoclimatol. Palaeoecol. 255, 267–283.

Hanor, J.S., 1994. Origin of saline fluids in sedimentary basins. In: Parnell, J. (Ed.), Geofluids: Origin, Migration and Evolution of Fluids in Sedimentary Basins. Geological Society (London) Special Publication, 78, pp. 151–174.

Hanor, J.S., 2000. Barite–celestine geochemistry and environments of formation. Rev. Mineral. Geochem. 40, 193–275.

Hanor, J.S., 2004. A model for the origin of large carbonate and evaporite-hosted celestine ($SrSO_4$) deposits. J. Sediment. Res. 74, 168–175.

Hodell, D.A., Mueller, P.A., Garrido, J., 1991. Variations in the strontium isotopic composition of seawater during the Neogene. Geology 19, 24–27.

Horita, J., Zimmermann, H., Holland, H.D., 2002. The chemical evolution of seawater during the Phanerozoic. Implications from the record of marine evaporites. Geochim. Cosmochim. Acta 66, 3733–3756.

Kaplan, I.R., Rittenberg, S.C., 1964. Microbial fractionation of sulphur isotopes. J. Soc. Gen. Microbiol. 34, 195–212.

Kesler, S.E., Jones, L.M., 1981. Surfur- and strontium-isotopic geochemistry of celestite, barite and gypsum from the Mesozoic basins of North-Eastern Mexico. Chem. Geol. 31, 211–224.

Kobluk, D.R., Crawford, D.R., 1990. A modern hypersaline organic mud- and gypsum-dominated basin and associated microbialites. Palaios 5, 134–148.

Lloyd, R.M., 1968. Oxygen isotope behavior in the sulphate–water system. J. Geophys. Res. 73, 6099–6110.

López-Chicano, M., Pulido-Bosch, A., 1995. Los manantiales termominerales de Salar (Granada). Un sistema de flujo profundo ligado esencialmente a la descarga de Sierra Gorda. Geogaceta 18, 138–141 (in Spanish).

López-Chicano, M., Cerón, J.C., Vallejos, A., Pulido-Bosch, A., 2001. Geochemistry of thermal springs, Alhama de Granada (southern Spain). Appl. Geochem. 16, 1153–1163.

Lowenstein, T.K., Risacher, F., 2009. Closed basin brine evolution and the influence of Ca–Cl inflow waters: Death Valley and Bristol Dry Lake California, Qaidam Basin, China, and Salar de Atacama, Chile. Aquat. Geochem. 15, 71–94.

Lowenstein, T.K., Timofeeff, M.N., Brennan, S.T., Hardie, L.A., Demicco, R.V., 2001. Oscillations in Phanerozoic seawater chemistry: evidence from fluid inclusion compositions in salt deposits. Science 294, 1086–1088.

Martín, J.M., Ortega-Huertas, M., 1986. Excursion to evaporites and associated strontium deposits of the Granada basin. In: Fenoll Hach-Ali, P. (Ed.), Geochemistry of the Earth Surface and Processes of Mineral Formation. Excursion Guidebook. Servicio de Publicaciones de la Universidad de Granada, pp. 1–17.

Martín, J.M., Ortega-Huertas, M., Torres-Ruiz, J., 1984. Genesis and evolution of strontium deposits of the Granada Basin (southeastern Spain): evidence of diagenetic replacement of stromatolite belt. Sediment. Geol. 39, 281–298.

McArthur, J.M., Howarth, R.J., Bailey, T.R., 2001. Strontium isotope stratigraphy: LOWESS version 3: best fit to the marine Sr-isotope curve for 0–509 Ma and accompanying look-up table for deriving numerical age. J. Geol. 109, 155–170.

Olaussen, S., 1981. Formation of celestite in the Wenlock, Oslo region, Norway — evidence for evaporitic depositional environments. J. Sed. Petrol. 51, 37–46.

Oliveri, E., Neri, R., Bellanca, A., Riding, R., 2010. Carbonate stromatolites from a Messinian hypersaline setting in the Caltanisseta Basin, Sicily: petrographic evidence of microbial activity and related stable isotope and rare earth element signatures. Sedimentology 57, 142–161.

Oren, A., Kühl, M., Karsten, U., 1995. An endoevaporitic microbial mat within gypsum crust: zonation of phototrophs, photopigments, and light penetration. Mar. Ecol. Prog. Ser. 128, 151–159.

Ortega-Huertas, M., Arana-Castillo, R., Rodríguez-Gallego, M., 1974. Observaciones mineralógicas y geoquímicas sobre el yacimiento de estroncio de Montevive (Granada). Cuad. Geol. 5, 5–19 (in Spanish).

Ortí, F., Pueyo, J.J., Geisler-Cussey, D., Dulau, N., 1984. Evaporitic sedimentation in the coastal salinas of Santa Pola (Alicante, Spain). Rev. Investig. Geol. 38 (39), 169–220.

Panieri, G., Lugli, S., Manzi, V., Roveri, M., Schreiber, B.C., Palinska, A., 2010. Ribosomal RNA fragments from fossilized cyanobacteria identified in primary gypsum from the late Miocene, Italy. Geobiology 8, 101–111.

Parkhurst, D.L., Appelo, C.A.J., 1999. User's guide to PHREEQC (versión 2). A computer program for speciation, batch-reaction, one dimensional transport, and inverse geochemical calculations. U.S. Geological Survey Water-Resources Investigations Report 99-4259 (312 pp.).

Parkhurst, D.L., Appelo, C.A.J., 2005. http://www.brr.cr.usgs.gov.

Paytan, A., Kastner, M., Campbell, D., Thiemens, M.H., 1998. Sulfur isotopic composition of Cenozoic seawater sulfate. Science 282, 1459–1462.

Petrash, D.A., Gingras, M.K., Lalonde, S.V., Orange, F., Pecoits, E., Konhauser, K.O., 2012. Dynamic controls on accretion and lithification of modern gypsum-dominated thrombolites, Los Roques, Venezuela. Sediment. Geol. 245–246, 29–47.

Pierre, C., 1985. Isotopic evidence for the dynamic redox cycle of dissolved sulphur compounds between free and interstitial solutions in marine salt pans. Chem. Geol. 53, 191–196.

Rees, C.E., 1973. A steady-state model for isotope fractionation in bacterial reduction processes. Geochim. Cosmochim. Acta 37, 1141–1162.

Riding, R., 2000. Microbial carbonates: the geological record of calcified bacterial–algal mats and biofilms. Sedimentology 47, 179–214.

Rodríguez-Fernández, J., Sanz de Galdeano, C., 2006. Late Orogenic intramontane basin development: the Granada basin, Betics (southern Spain). Basin Res. 18, 85–102.

Rouchy, J.M., 1982. La genèse des évaporites messiniennes de Méditerranée. 50. Mémories du Muséum National d'Histoire Naturelle (267 pp.).

Rouchy, J.M., Monty, C., 1981. Stromatolites and cryptalgal laminites associated with Messinian gypsum of Cyprus. In: Monty, C. (Ed.), Phanerozoic Stromatolites. Springer, Berlin–Heidelberg–New York, pp. 182–225.

Rouchy, J.M., Monty, C., 2000. Gypsum microbial sediments: Neogene and modern examples. In: Riding, R., Awramik, S.M. (Eds.), Microbial Sediments. Springer-Verlag, Berlin Heidelberg, pp. 209–216.

Rouchy, J.M., Pierre, C., 1979. Données sédimentologiques et isotopiques sur gypses des séries évaporitiques messiniennes d'Espagne méridionale et de Chypre. Rev. Géol. Dynam. Géog. Phys. 21, 267–280 (in French).

Sanz de Galdeano, C., 2008. The Cádiz–Alicante Fault: an important discontinuity in the Betic Cordillera. Rev. Soc. Geol. Esp. 21, 49–58.

Sanz de Galdeano, C., Ortega-Huertas, M., Arana-Castillo, R., 1976. Nuevo yacimiento de celestina en la Depresión de Granada. Estudio geológico y mineralógico. Estud. Geol. 32, 435–442 (in Spanish).

Scholle, P.A., Stemmerik, L., Harpoth, 1990. Origin of major karst-associated celestine mineralization in Karstrynggen, Central East Greenland. J. Sediment. Petrol. 60, 397–410.

Schreiber, B.C., 1978. Environments of sub-aqueous evaporites. In: Dean, W.E., Schreiber, B.C. (Eds.), Marine Evaporites. SEPM Short Course 4, Oklahoma City, pp. 1–5.

Taberner, C., Marshall, J.D., Hendry, J.P., Pierre, C., Thirlwall, M.F., 2002. Celestite formation, bacterial sulphate reduction and carbonate cementation of Eocene reefs and basinal sediments (Igualada, NE Spain). Sedimentology 49, 171–190.

Tekin, E., Varol, B., Friedman, G.M., 2001. A preliminary study: celestite-bearing gypsum in the Tertiary Sivas Basin, Central-Eastern Turkey. Carbonates Evaporites 16, 93–101.

Tekin, E., Varol, B., Sayili, I.S., 2002. Indications of intermediate compositions in the $BaSO_4$–$SrSO_4$ solid-solutions series from the Bahçeciktepe celestine deposit, Sivas, East-Central Anatolia, Turkey. Can. Mineral. 40, 895–908.

Thode, H.G., 1991. Sulphur isotopes in nature and environment: an overview. In: Krouse, H.R., Grinenko, V.A. (Eds.), Stable Isotopes in Assessment of Natural and Anthropogenic Sulphur in the Environment. Wiley and Sons Ltd., pp. 1–26.

Thode, H.G., Monster, J., 1965. Surfur-isotope geochemistry of petroleum evaporites and ancient seas. AAPG Bull. 4, 363–373.

Thomas, J.C., 1984. Formations benthiques à Cyanobactéries des salins de Santa Pola (Espagne): composition spécifique, morphologie et caractéristiques biologiques des principaux peuplements. Rev. Investig. Geol. 38 (39), 139–158 (in French).

Vai, G.B., Ricci-Lucchi, F., 1977. Algal crusts, autochthonous and clastic gypsum in a cannibalistic evaporite basins: a case history from the Messinian of Northern Apennines. Sedimentology 24, 211–244.

Veizer, J., Ala, D., Azmy, K., Bruckschen, P., Buhl, D., Bruhn, F., Garden, G.A.F., Diener, A., Ebneth, S., Godderis, Y., Jasper, T., Korte, Ch., Pawellek, F., Podlaha, O.G., Strauss, H., 1999. $^{87}Sr/^{86}Sr$, $\delta^{13}C$ and $\delta^{18}O$ evolution of Phanerozoic seawater. Chem. Geol. 30, 59–88.

Vogel, M.B., Des Marais, D.J., Parenteau, M.N., Jahnke, L.L., Turk, K.A., Kubo, M.D.Y., 2010. Biological influences on modern sulfates: textures and composition of gypsum deposits from Guerrero Negro, Baja California Sur, Mexico. Sediment. Geol. 223, 265–280.

West, I.M., 1960. On the occurrence of the celestine in the Caps and Broken Beds at Durlston Head, Dorset. Proc. Geol. Assoc. 71, 391–401.

Wood, M.W., Shaw, H.F., 1976. The geochemistry of celestites from the Yate area near Bristol (U.K.). Chem. Geol. 17, 179–193.

Zherebstova, I.K., Volkova, N.N., 1966. Experimental study of behavior of trace elements in the process of natural solar evaporation of Black Sea water and Sasyk–Sivash brine. Geochem. Int. 7, 656–670.